

1 Relationship between structures, stress and
2 seismicity in the Charlevoix seismic zone revealed by
3 3-D geomechanical models: Implications for the
4 seismotectonics of continental interiors

A. F. Baird, S. D. McKinnon, and L. Godin

5 Department of Geological Sciences and Geological Engineering, Queen's
6 University, Kingston, Ontario, Canada

A. F. Baird, L. Godin, and S. D. McKinnon, Department of Geological Sciences and Geological Engineering, Queen's University, Kingston, Ontario, Canada K7L 3N6. (baird@geol.queensu.ca; godin@geol.queensu.ca; sm@mine.queensu.ca)

7 **Abstract.** The Charlevoix seismic zone in the St. Lawrence valley of Québec
8 is the most active in eastern Canada. The structurally complex region com-
9 prises a series of subparallel steeply dipping Iapetan rift faults, superimposed
10 by a 350 Ma meteorite impact structure, resulting in a heavily faulted vol-
11 ume. The elongate seismic zone runs through the crater parallel to the rift.
12 Most large events localize outside the crater and are consistent with slip along
13 the rift faults, whereas background seismicity primarily occurs within the
14 volume of rock bounded by the rift faults within and beneath the crater. The
15 interaction between rift and crater faults is explored using the three-dimensional
16 stress analysis code FLAC3D. The rift faults are represented by frictional
17 discontinuities and the crater by a bowl-shaped elastic volume of reduced
18 modulus. Differential stresses are slowly built up from boundary displace-
19 ments similar to tectonic loading. Results indicate that weakening the rift
20 faults produces a stress increase in the region of the crater bounded by the
21 faults. This causes a decrease in stability of optimally oriented faults, and
22 may explain the localization of low-level seismicity. Additionally, slip distri-
23 bution along the rift faults shows that large events localize at the perime-
24 ter of the crater and produce focal mechanisms with P-axes oblique to the
25 applied stress field, consistent with historic large earthquakes. It is specu-
26 lated that similar systematic rotation of focal mechanism P-axes may be ex-
27 pected along other intraplate rift zones, raising a potential caveat for the use
28 of focal mechanisms for stress estimation in continental interiors.

1. Introduction

29 The Charlevoix seismic zone (CSZ) in the St. Lawrence valley of Québec is the most
30 seismically active region in eastern Canada (Figure 1). It has been the site of several
31 large historic events (five moment magnitude $M > 6$ events since 1663) [*Adams and*
32 *Basham*, 1991] as well as continuous low-level activity. Like most intraplate earthquake
33 zones, the cause of the focus of seismic activity is not well understood. On a broad scale,
34 intraplate seismicity is often associated with pre-existing weak structures such as ancient
35 rift zones and aulacogens [e.g. *Sykes*, 1978]; however, small areas of intense activity are
36 often attributed to local effects. The CSZ lies at the intersection of two potential sources
37 of weakness; the Cambro-Ordovician St. Lawrence rift, which strikes NE-SW along the
38 river, and the Charlevoix Impact structure, which is a large bowl shaped damage zone
39 formed as a result of a meteorite impact ~ 300 Ma [*Rondot*, 1971].

40 The relative importance of the two structures in the distribution of seismicity has been
41 debated. *Leblanc et al.* [1973], noting several small events coinciding with the location
42 of large past events and a meteorite crater, proposed that weakened crust caused by the
43 impact could yield more easily to postglacial strain. Extensive microseismic monitoring
44 further delineated the extent of the seismic zone, and revealed that there were in fact two
45 clusters of seismicity running along the length of the St. Lawrence, which coincide with
46 the interpreted location of rift faults [*Anglin*, 1984]. This information, combined with
47 an absence of seismicity at other Canadian meteorite craters, led *Adams and Basham*
48 [1991] to attribute the earthquakes to the reactivation of rift faults, possibly weakened
49 by the crater. Improvements in hypocenter location and analysis of microseismicity focal

50 mechanisms in the 1990's however, has revealed that much of the seismicity clusters are
51 not occurring along planar structures, but appear to be located in fractured volumes of
52 rock bounded by the major rift faults [*Lamontagne*, 1999]. Thus both the impact structure
53 and the rift faults appear to play an important role in the distribution of seismicity in the
54 CSZ.

55 While much has been published describing the seismicity in the CSZ, little work has been
56 done to explain the mechanics behind the partitioning of seismicity. *Baird et al.* [2009],
57 addressing this with simple 2-D stress models, showed that a series of parallel weak faults
58 intersecting a 'soft zone' can act as a stress conduit, channeling background stresses into
59 the interior of the weak zone, which would otherwise simply flow around it. The models
60 were used to illustrate this concept as a way to explain much of the background seismicity
61 patterns observed in the CSZ. The models, however, had a number of limitations, primarily
62 brought on by the restriction to two dimensions. The current study builds on the results
63 of *Baird et al.* [2009] by extending the models to three dimensions in order to better
64 represent the true 3-D architecture of the system. In addition to corroborating the results
65 of the 2-D models, the 3-D models are used to explain the extension of earthquakes below
66 the crater, address slip along the rift faults themselves, which appear to form the locus of
67 the less frequent large events, and provide evidence for a misfit between focal mechanism
68 P-axes and the orientation of maximum horizontal compressive stress S_H .

2. Background

2.1. Geologic setting

69 The CSZ lies in a structurally complex setting created by a series of tectonic events
70 spanning the last 1.1 billion years (Figure 2a). The oldest tectonic episode recorded in

71 the region consists of the 1100-990 Ma Grenville orogeny, which resulted from a series
72 of exotic terranes accreting onto the southeast margin of Laurentia [*Rivers, 1997*]. The
73 upper amphibolite to granulite metamorphic facies rocks of the Grenville Province make
74 up the core of this orogen and now form the basement of the Charlevoix area (Figure 2b).
75 Following a period of erosion the area was subjected to a late Proterozoic to early Pa-
76 leozoic rifting event associated with the breakup of the Rodinia supercontinent and the
77 formation of the Iapetan Ocean [*Kumarapeli, 1985*]. A series of normal faults forming the
78 St. Lawrence paleo-rift system represented the passive margin of the proto-North Amer-
79 ican continent onto which carbonate rocks of the St. Lawrence platform were deposited
80 [*St-Julien and Hubert, 1975*]. The next major tectonic phase was associated with the
81 closing of the Iapetan Ocean and the formation of the Appalachian orogen. Appalachian
82 Nappes were thrust over the North American continent as far west as the St. Lawrence
83 in the Charlevoix area. The deformation front, known as Logan's Line, runs through the
84 CSZ [*Rondot, 1994*]. Following this, in the Devonian (~ 350 Ma) the region was subjected
85 to a meteorite impact resulting in a large (~ 56 km diameter) crater [*Rondot, 1971*]. The
86 last significant tectonic episode to effect the region was the normal sense reactivation of
87 the Iapetan rift faults due to the opening of the Atlantic in the Mesozoic [*Lemieux et al.,*
88 2003].

89 Since the Appalachian Nappes are confined to the upper few kilometers, and most
90 of the seismicity is located in the deeper Grenville basement rocks, the most pertinent
91 structural features are the rifted faults and the impact structure (Figure 2b). The NE-
92 SW trending St. Lawrence rift is a half-graben represented by a series of parallel normal
93 faults steeply dipping to the SE, which extend into the Grenville basement [*Tremblay*

94 *et al.*, 2003]. In the Charlevoix region these faults include the Gouffre North-West and St.
95 Laurent faults that parallel the St. Lawrence river along its north shore, the Charlevoix
96 fault, which lies under the river, and the South Shore fault, which does not outcrop on the
97 surface but is inferred from gravity and magnetic data [*Lamontagne*, 1999](Figure 2a,b).

98 The Charlevoix impact structure forms a ~ 56 km diameter damaged zone exhibiting
99 varied fault orientations. The faults include a polygonal ring graben system between 16
100 and 20 km from the center [*Rondot*, 1994] in which rocks of the St. Lawrence platform
101 are locally preserved (Figure 2). In the interior portion of the crater the faults are more
102 scattered in orientation [*Lemieux et al.*, 2003]. Faulting associated with the crater is
103 estimated to extend to a depth of approximately 12 km [*Rondot*, 1994].

2.2. Seismicity

104 The CSZ has been the locus of five earthquakes greater than **M** 6 in recent history (in
105 1663, 1791, 1860, 1870, and 1925) [*Adams and Basham*, 1991]. The site is also host to
106 an abundance of background seismicity. Over 200 events are recorded each year, most
107 of which are lower than Nuttli magnitude (m_N) 3.0. Earthquakes occur almost entirely
108 within the Grenville basement, with most activity between 7–15 km depth, but with some
109 as deep at 30 km (Figure 2c).

110 The spatial distribution of the background seismicity appears to be largely controlled
111 by the St. Lawrence rift and the impact structure. The seismically active region spans
112 approximately 30 by 85 km covering the area of overlap between the two structures and
113 extending beyond the boundaries of the crater along the rift to the northeast (Figure 2a).
114 A cross-sectional view of the seismicity across the strike of the rift reveals that earthquakes
115 cluster into two distinct elongate zones, with the northwest cluster steeply dipping to

116 the southeast (Figure 2b). The similarity in orientation of these clusters with the St.
117 Lawrence rift faults led *Anglin* [1984] to conclude that most of the seismicity was related to
118 reactivation of the faults. Improvements in hypocenter locations over the years, however,
119 combined with evidence of varied slip planes from microseismic focal mechanisms suggest
120 that much of the activity is not located on the major faults but within a fractured volume
121 bounded by the rift faults [*Lamontagne*, 1999].

122 Although the active region of the CSZ extends beyond the boundaries of the crater,
123 most of the low magnitude background activity occurs either within or beneath it (Fig-
124 ures 2c and 3). The large increase in shallow events within the crater area relative to
125 the surrounding regions is strongly suggestive of its influence on the seismicity of the
126 area. This is unusual, however, since most large impact structures found worldwide are
127 seismically inactive [*Solomon and Duxbury*, 1987].

128 While the impact structure appears to be strongly associated with low-level background
129 seismicity, the opposite is true for larger events. As shown in Figure 2, all events larger
130 than m_N 4.0 (red circles) since 1985 have occurred outside the crater, with most clustering
131 at the northeast end. Additionally most large events over the last century have occurred
132 to the northeast of the crater, including the 1925 M 6.2 event and the 1979 m_N 5.0 event
133 [*Hasegawa and Wetmiller*, 1980; *Bent*, 1992]. Bearing in mind that the rupture surface
134 of events of this magnitude are estimated to be on the order of several kilometers wide
135 [*Johnston*, 1993], the localization of large events outside the crater as well as a common
136 SE dipping nodal plane (Figure 4) suggest that the rift faults form the locus of these large
137 events.

2.3. Stress Field

138 The CSZ is located within the Midplate stress province of eastern North America,
139 which is dominated by NE- to ENE- oriented maximum horizontal compressive stress
140 (S_H) [Zoback and Zoback, 1991]. Plate-driving forces from the mid-Atlantic ridge likely
141 provide the greatest source of stress [Richardson and Reding, 1991; Adams and Bell, 1991;
142 Zoback and Zoback, 1991]. The orientation of the stress field is inferred from a variety
143 of data sources, which have been included in the World Stress Map database. In eastern
144 Canada and the northeastern United States these are primarily borehole breakouts and
145 earthquake focal mechanisms [Heidbach *et al.*, 2008].

146 Borehole breakout data from the World Stress Map database for southeastern Canada
147 are shown in Figure 1. These include a large number of measurements along the St.
148 Lawrence river approximately 100–250 km southwest of the CSZ, between Québec City
149 and Montréal, which are all consistently oriented NE-SW, subparallel to the river.

150 Earthquake focal mechanisms provide another source of stress data where the P, B,
151 and T axes are used to provide an estimate of the principal stress orientations [Zoback,
152 1992a]. However, P and T axes can potentially differ significantly from the actual stress
153 orientations with the only strict constraint being that the orientation of the major prin-
154 cipal stress must lie within the dilatational field of the focal mechanism [e.g. McKenzie,
155 1969]. Consequently it is current practice that all stress orientations inferred from indi-
156 vidual focal mechanisms are given a quality ranking of no more than C ($\pm 25^\circ$ uncertainty)
157 regardless of how well the mechanism is constrained [Barth *et al.*, 2008]. Despite these
158 problems, focal mechanisms do provide some constraint on the stress orientation and also
159 contain useful information on the geometry of fault slip.

160 A case study was carried out by *Zoback* [1992b], examining the focal mechanisms of
161 32 moderate earthquakes in eastern North America to determine whether slip was com-
162 patible with the regional stress field. A similar study by *Du et al.* [2003] supplemented
163 the data with 16 more moderate events since 1990. Of the events examined, most were
164 broadly compatible with the regional stress field, with NE-SW oriented P-axes. However,
165 there were a few notable exceptions, including four events located along the St. Lawrence
166 river (two from the CSZ), which had P-axes oriented NW-SE (Figure 1). *Zoback* [1992b]
167 found that while the 1979 Charlevoix earthquake was geometrically possible in the in-
168 ferred regional stress field, it was frictionally unlikely, requiring either very weak faults or
169 superlithostatic pore pressure. Alternatively it was argued that it was related to a local
170 stress perturbation, possibly due to the presence of a dense rift pillow beneath the St.
171 Lawrence [*Zoback*, 1992b]. Similar models have been proposed to explain the earthquake
172 concentration in the New Madrid seismic zone in the central United States, which is lo-
173 cated within the Reelfoot rift [*Grana and Richardson*, 1996], and to explain an apparent
174 stress rotation near the Amazonas rift in Brazil [*Zoback and Richardson*, 1996]. Published
175 studies, however, are insufficient to support or refute the existence on a rift pillow beneath
176 the St. Lawrence [*Du et al.*, 2003]. These models also fail to account for the large number
177 of borehole breakout data indicating rift parallel compression between Québec City and
178 Montréal (Figure 1).

179 One of the major shortcomings of these broad regional focal mechanism studies is the
180 limited datasets used. All four of the anomalous events examined along the St. Lawrence
181 were larger than **M** 4. Examining a variety of focal mechanisms from the CSZ, however,
182 reveals that while larger events ($m_N > 4$) typically have NW-SE oriented P-axes, smaller

183 events are considerably more varied (Figure 4). A formal stress inversion of 60 focal
184 mechanisms carried out by *Mazzotti and Townend* [2010] yields a S_H orientation of 086°
185 for the whole of the CSZ, an approximately 30° clockwise rotation from S_H inferred
186 from borehole measurements. A more detailed analysis into spatial variations of stress
187 within the CSZ, however, reveals two distinct estimates of S_H orientation between events
188 clustering northwest of the Saint-Laurent fault versus those from the southeast (Figure 4).
189 A 47° apparent rotation exists between the two groups, with the NW cluster roughly
190 parallel to the borehole data and the rift trend, and the SE cluster strongly oblique to it
191 [*Mazzotti and Townend*, 2010].

192 The significance of the large apparent rotation between the borehole and focal mech-
193 anism inferred S_H orientations is not clear at this time. However, the variations in S_H
194 derived from microseismicity from within the CSZ suggest that it is a very localized effect
195 and likely not due to a regional stress perturbation. Discussion of possible mechanisms
196 causing the rotation is addressed later in this paper.

3. Numerical Approach

197 *Baird et al.* [2009] used a 2-D stress analysis code to investigate the interaction between
198 the rift faults and crater by locally altering the regional stress field and controlling the
199 distribution of seismicity. In this paper we take a similar approach using the 3-D code
200 FLAC3D (Fast Lagrangian Analysis of Continua) [*Itasca Consulting Group Inc.*, 2005].
201 FLAC3D uses finite difference techniques to compute stress and strain within discretized
202 continuum blocks while permitting the inclusion of a small number of discontinuities to
203 represent discrete faults.

204 The main reason for using a 3-D code is to better represent the true architecture of
205 the system and to allow oblique slip displacements along modeled faults, which were
206 previously restricted to strike-slip. For simplicity we limit the structures included to only
207 those features which play an important role in the distribution of seismicity, namely the rift
208 faults and the impact crater (Figure 5). The rift faults are represented as a series of three
209 parallel frictional discontinuities striking at N035° and steeply dipping to the southeast.
210 Due to difficulty in including curved interfaces to model listric faults, the models are tested
211 with fault dips of 60° and 70°. The faults roughly correspond to the Gouffre North-West,
212 Saint-Laurent and South Shore faults, which appear to form the main boundaries of the
213 seismicity (Figure 2). The Impact structure is represented in the models as the lower half
214 of an oblate spheroid, with a 30 km radius at the surface and extending to a depth of
215 15 km below the center. Rather than represent the complex faulted volume with explicit
216 faults, the damaged volume is simulated by using a continuum of lowered elastic modulus
217 following the well established concept of an equivalent continuum for fractured rock [e.g.
218 *Fossum*, 1985].

3.1. Initial and boundary conditions

219 An elastic continuum constitutive model is chosen to represent the crust in which den-
220 sity, bulk, and shear moduli must be prescribed. Density is assumed to be 2700 kg m⁻³,
221 typical of upper crustal rock. The background moduli for the region outside the crater
222 (both bulk and shear, hereby denoted collectively as M_B) is derived from P and S-wave
223 velocity models for the Saguenay region to the north of the CSZ [*Somerville et al.*, 1990].
224 The variation of M_B with depth is shown in Figure 6a. Within the crater, the elastic mod-
225 ulus values (denoted M_C) are lowered to simulate the damaged zone. Since the equivalent

226 modulus is not known it was tested at 1/4 and 1/2 the value of the surrounding rock
227 (M_B).

228 Eastern Canada is characterized by a triaxial thrust regime state of stress (i.e. $S_H >$
229 $S_h > S_V$) [Adams and Bell, 1991]. However, rather than initializing a differential stress in
230 the models, a simple lithostatic stress field is initialized, and the horizontal compressive
231 stress is then slowly increased through boundary displacements. This procedure ensures
232 compatibility between the stresses and fault displacement. Since it is assumed that the
233 largest contribution to stress in the region is from far-field tectonic sources, boundary
234 displacements are applied in the direction of tectonic loading over a series of computational
235 time steps. The stress field is slowly built up until the differential stress at a depth of
236 10 km is approximately 200 MPa (Figure 6b), which is of the same order of estimates of
237 stress differences at that depth [e.g. Hasegawa et al., 1985; Zoback et al., 1993; Lamontagne
238 and Ranalli, 1996].

3.2. Processing technique

239 The main purpose of the modeling is to understand the partitioning and distribution of
240 seismicity. For this, we distinguish two classes of earthquakes: (a) Earthquakes that occur
241 off the main rift faults, on fractures and minor faults that are not explicitly modeled, and
242 (b) Earthquakes that nucleate along the major rift faults, which are explicitly included.
243 We use different techniques to interpret the two classes of events.

244 **Earthquakes off the rift faults:** Events located away from the rift faults constitute
245 the bulk of the low-level background seismicity that is observed in the CSZ, which are
246 interpreted to cluster within fractured volumes bounded by the rift faults. Because the
247 faults associated with these events are not explicitly included in the models, their stability

248 must be inferred using alternative means. A useful parameter for inferring fault stability is
 249 differential stress (σ_D) which is proportional to maximum shear stress. Differential stress
 250 is defined as the difference in magnitude between the major and minor principal stresses:

$$251 \quad \sigma_D = \sigma_1 - \sigma_3 \quad (1)$$

252 The presence of a high differential stress alone, however, does not necessarily lead to
 253 seismic activity. Other factors, such as confining pressure and the availability of optimally
 254 oriented fractures also play an important role. However, within a homogeneous randomly
 255 fractured rockmass an *increase* in differential stress would be expected to produce an
 256 increased incidence of seismicity. If there is no preferred fault orientation then stress
 257 release would be expected to be distributed over a variety of small faults rather than a
 258 large event on a single fault.

259 For the Charlevoix model analysis, a control model is first developed that acts as a point
 260 of comparison for other models. Most large impact structures are seismically inactive
 261 [Solomon and Duxbury, 1987], and much of the background seismicity within the crater
 262 is thought to be the result of interaction with the rift faults. Consequently a suitable
 263 control model is one in which the rift faults are omitted and only the impact structure
 264 is modeled. Further models which incorporate weak rift faults can then be compared
 265 directly to the control model, which is assumed to be aseismic. For the analysis we define
 266 a new parameter $\Delta\sigma_D$:

$$267 \quad \Delta\sigma_D = \frac{\sigma_{Dmodel} - \sigma_{Dcontrol}}{\sigma_{Dcontrol}} \quad (2)$$

268 where σ_{Dmodel} and $\sigma_{Dcontrol}$ indicate the differential stress magnitude within a test model
 269 and the control model, respectively, for a common discretized zone. A positive value of

270 $\Delta\sigma_D$ indicates regions which have had an increase in differential stress relative to the
271 assumed aseismic control model, and thus an increase in the potential for earthquakes to
272 occur. Conversely a negative value of $\Delta\sigma_D$ would suggest a reduction in seismicity.

273 **Earthquakes on the rift faults:** Unlike the faults of the impact structure, the
274 regional-scale rift faults are explicitly included in the models as discontinuities that are
275 assigned Mohr-Coulomb frictional strength parameters. Fault stability can therefore be
276 inferred simply by monitoring slip activity as the background differential stress is built
277 up through boundary displacements. The build up of the stress in the model is done over
278 10,000 computational time-steps (not linked to true time). To monitor temporal changes
279 in slip activity a 100 step interval is arbitrarily chosen to represent a “small” amount of
280 time. Relative slip displacement accumulated over the interval is then calculated for each
281 fault gridpoint and plotted as a vector field indicating both magnitude and direction of
282 slip of the hanging wall relative to a stable footwall. By viewing these vector fields as a
283 time sequence, temporal variations in slip activity on the rift faults and their relationship
284 to along-strike structural variations can be observed.

4. Results

4.1. Seismicity off the rift faults

285 To analyze the stress models for seismicity off the main faults, the data are processed
286 to calculate the change in differential stress ($\Delta\sigma_D$) caused by weak rift faults as defined in
287 equation 2. Using this definition, positive values are expected to indicate regions where
288 seismicity is promoted, particularly in areas where pre-existing faults and fractures occur,
289 such as in the interior of the crater. Figure 7 shows a series of sectional contour plots of
290 this value, showing its 3-D distribution through a model with $M_C = 1/4M_B$, weak rift

291 faults with a friction angle of 5° , and an applied regional orientation of S_H of $N050^\circ$ as
292 inferred from borehole measurements [*Heidbach et al.*, 2008].

293 At the shallower levels within the depth range of the crater (5 km and 10 km, Figure 7a),
294 there is a clear increase in differential stress in the region of the crater bounded by the
295 rift faults, which corresponds to the general pattern of background seismicity observed
296 in the CSZ (Figure 2a). At deeper levels (15 km and 20 km) a similar pattern exists,
297 although not as prominent as at shallow depths. Cross-sectional views, both across and
298 along strike (Figures 7b–d) show a pattern of increased stress concentrations between the
299 rift faults, both within and beneath the crater, which match the general 3-D pattern of
300 seismicity observed in the CSZ (Figure 2).

301 To understand the reason for these stress concentrations, the effect of the relevant struc-
302 tures on the pattern of regional stresses must be examined. When the crater is considered
303 on its own, without the influence of the rift, the trajectories of the major principal stress
304 tends to flow around the structure (Figure 8a). This leaves the mechanically weaker ma-
305 terial in the interior of the crater at a lower state of differential stress, thus diminishing
306 the probability of earthquakes. When weak rift faults are also included in the model
307 (Figure 8b), the largest effect is a local rotation of S_H such that it becomes more parallel
308 to the faults. While the effect of the re-orientation is subtle ($< 15^\circ$ rotation), it does dis-
309 rupt the pattern of stress around the crater such that higher concentrations of differential
310 stress form in the interior of the crater between the rift faults. In cross-section the major
311 principal axis of the stress field also flows beneath the crater, thus resulting in a higher
312 differential stresses in this area as well (Figure 8c).

313 The general pattern of stress partitioning is very similar to the main findings from
314 *Baird et al.* [2009]. However, the 3-D models reveal some additional details observed
315 in the CSZ that were not found in the 2-D models. One of the notable details of the
316 seismicity distribution is an extension of the active zone along the rift to the northeast
317 of the crater, while there is minimal background seismicity to the southwest (Figure 2).
318 A similar pattern of increased differential stress to the northeast of the crater is observed
319 in the model, most clearly at the 10 and 15 km depth sections (Figure 7a) and also
320 in the cross-sections along fault strike (Figure 7c). This effect is mainly a consequence
321 of the asymmetry imposed on the system by the inclination of the applied stress field
322 orientation relative to the rift fault orientation. This is illustrated in Figure 9 where the
323 differential stress changes are plotted for models with applied loading at N045°, N055°,
324 and N065° (equal to a 10°, 20° and 30° clockwise rotation from the strike of the rift).
325 When the applied stress is at low angles to the rift, the region of increased differential
326 stress extends out of the crater the most, however, the magnitude of this increase is low.
327 At higher angles the extension out of the crater is reduced, but stress concentration inside
328 the crater increases. An applied stress orientation of N050° as shown in Figure 7 forms a
329 pattern which best matches the observed seismicity patterns, and is consistent with the
330 inferred orientation of S_H from borehole breakout measurements [*Heidbach et al.*, 2008].

4.2. Seismicity on the rift faults

331 To analyze seismicity localized on the rift faults, the slip activity is monitored as stresses
332 are progressively built up through boundary displacements. While this is not strictly
333 equivalent to the build-up of tectonic stresses, it can be used to make some inferences of
334 the relative stability of different portions of the faults. The behavior is best observed by

335 viewing the animations provided in the supplementary material¹. Figure 10 shows a vector
336 field of the hangingwall shear displacement relative to a stable footwall for: (a) All three
337 faults over a small time interval during the progressive boundary displacement and (b) a
338 closeup of the northern fault at the northeastern side of the crater before (top), during
339 (middle) and after (bottom) the activity shown in part (a). At early times the stress field
340 is effectively lithostatic and there is little motion along the faults. As differential stress
341 is built up, the induced strain begins to be accommodated by fault slip, with most initial
342 activity localized near the surface and then gradually migrating deeper. Inside the crater
343 the amount of rift fault slip is noticeably lower than the activity outside. The focus of slip
344 activity outside the crater migrates over time, showing a cyclical pattern where activity
345 builds up on the northeast before decreasing to a background level and then increasing to
346 the southwest of the crater. The maximum slip magnitude during these pulses of activity
347 occurs just outside the perimeter of the crater (Figure 10a and b middle).

348 The slip partitioning along the rift faults appears to be largely the consequence of the
349 modulus contrast between the crater and the surrounding rock. The rift faults represent
350 a large-scale regional weak zone within a relatively strong crust. As a consequence of
351 this, much of the far-field strain is accommodated by concentrated deformation along the
352 rift. Along most of its extent the rift is surrounded by relatively stiff rocks, favoring slip
353 along the discrete bounding faults. Where the rift passes through the crater there is a
354 noticeable decrease in slip activity along the faults, and there is a corresponding increase
355 of stress within the crater as a result of its interaction with the weak rift faults (Figure 7).
356 This suggests that the decrease of fault slip is simply due to the transition from strain
357 accommodation by discrete fault slip along the rift boundary faults to accommodation by

358 bulk deformation where the rift passes through the damaged impact zone. The periodic
359 large slip activity just outside the crater boundaries appears to be caused by the build up
360 of shear stress on these faults due to the flow of stress around the crater (Figure 8).

4.3. Stress and focal mechanisms

361 Perhaps the most puzzling aspect of the CSZ is the apparent inconsistencies in the
362 inferred orientation of stress. Focal mechanism based stress inversions suggest that stress
363 is oriented parallel to the rift in the NW cluster of events, but strongly oblique to the rift in
364 the SE cluster (Figure 4) [*Mazzotti and Townend, 2010*]. Most available stress information
365 is derived from focal mechanisms of events from within the seismic zone, for comparison
366 purposes the modeled principal stress orientations from the approximate dimensions of
367 the seismic zone are plotted in Figure 11a. It shows stress orientations from all gridpoints
368 between the rift faults for depths shallower than 15 km between the southwest boundary
369 of the crater, to 30 km past the northeast boundary of the crater (Figure 11b). The figure
370 shows an orientation of S_H very similar to the applied loading directions. This matches
371 the inferred S_H orientation from the NW cluster of events, but it is inconsistent with
372 the SE cluster, which shows a strong ($\sim 45^\circ$) clockwise rotation (Figure 4)[*Mazzotti and*
373 *Townend, 2010*].

374 Focal mechanism parameters for events on the rift faults in the model are computed
375 using the fault geometry and slip vector data. Figure 11c shows a contour plot of the
376 modeled P, T and B axes in a lower hemisphere projection. The most notable characteristic
377 of this is the large ($\sim 35^\circ$) clockwise rotation of the P-axis orientation relative to the
378 direction of loading. The mechanism is similar in style to that of the large earthquakes
379 observed in the CSZ, although the natural events typically have a larger thrust component

380 than in the model. Figure 11d shows the resulting average mechanism if the fault dip is
381 lowered to 60° . This results in further rotation of the P-axis as well as a larger thrust
382 component, providing a better match to the focal mechanisms of the observed large events.
383 It is likely that some variation of fault dip with depth (i.e. listric faults) could account
384 for some variability in the observed style of mechanisms.

5. Discussion

385 The models are able to reproduce many of the observed seismicity characteristics of the
386 CSZ. The region of increased differential stress between the rift faults in the models shows
387 a remarkably similar pattern to the observed background seismicity (Figure 7), including
388 details such as the extension of the seismicity to the NE of the crater, which only occurs
389 when the applied boundary conditions are close the regional orientation of S_H as inferred
390 by borehole data. The comparatively soft impact crater is shown to influence the stability
391 of the rift faults intersecting it as it responds to regional strain from far-field boundary
392 displacements (Figure 8). Rift fault slip is significantly reduced within the crater, where
393 strain accommodation due to bulk deformation predominates (Figure 10). However, slip is
394 locally promoted just outside the boundaries of the crater (Figure 10b); this corresponds
395 spatially to the regions of large events observed in the CSZ (Figure 2). Additionally, the
396 sense of slip along the faults implies a significantly rotated P-axis compared to the applied
397 regional stress (Figures 11c and d), which is similar in style to the focal mechanisms of
398 large events at the CSZ (Figure 4).

399 Although the models do address the apparent stress field rotation observed when con-
400 sidering only large events, they do not adequately explain the difference in S_H orientation
401 between the two rift parallel clusters of seismicity (Figure 4)[*Mazzotti and Townend, 2010*].

402 These stress orientations were calculated by a formal stress inversion technique using both
403 large and small events. The difference between the model results and observations may
404 be partially explained by considering the implications of some of the structural simpli-
405 fications made in the model. The three large rift faults are the only true failure planes
406 included in the models. All other material is represented by an isotropic continuum. The
407 impact crater in reality is a complex faulted structure, which is simulated by representing
408 the damaged zone as a continuum with reduced elastic properties. However, in doing so,
409 much of the complexity is removed. The reduced elastic modulus representation is likely
410 most valid in the central portion of the crater, which is characterized by a wide scat-
411 tering of fracture orientations [Lemieux *et al.*, 2003]. In the outer portion of the crater,
412 fault geometry is dominated by a ring graben structure, such that the prominent fault
413 orientation is roughly parallel to the boundary [Rondot, 1994]. Mechanisms from the NW
414 cluster yielded a S_H orientation roughly parallel to the regional field (Figure 4). This
415 is encouraging, as this cluster runs through the center of the crater, where the isotropic
416 representation is likely more valid given the scattered orientation of fractures. The SE
417 cluster, however, yielded a S_H orientation strongly oblique to the rift, similar to the P-
418 axis orientation from large events [Mazzotti and Townend, 2010]. It is notable that this
419 cluster occurs near the southeast boundary of the crater, where crater faults are likely to
420 be preferentially oriented NE-SW similar to the rift faults. Perhaps more importantly, a
421 large number of the focal mechanisms in this cluster extend beneath the lower boundary
422 of the crater, into the rifted crust below (Figure 4c). In the models the rift is represented
423 as three discrete faults, with no structure in the rocks between them. In reality these
424 rocks likely exhibit minor faulting in a similar style to the regional faults, and thus have

425 a prominent NE-SW orientation. The rifted block beneath the crater is still affected by a
426 differential stress concentration due to the stress deflection beneath the crater; however,
427 by analogy with the larger events, much of the minor event focal mechanisms in this area
428 would be expected to reflect the local structure.

429 One troubling requirement of the models is that the regional rift faults must be very
430 weak, as they are poorly oriented for reactivation in the regional stress field. This weakness
431 can be due to an unusually low frictional strength (as was used in the model), a very large
432 pore-fluid pressure, or by some combination of the two. While this is unusual it has been
433 proposed as a possible explanation for the large thrust events in the CSZ [e.g. *Zoback,*
434 *1992b; Du et al., 2003*]. *Lamontagne* [1999] proposed a model for the CSZ in which the
435 rift faults could act as a conduit for fluids under pressure, causing an inherent weakness.
436 Regardless of the source of fault weakness, its effect in the models leads to the formation
437 of patterns of stress and seismicity compatible with observations.

6. Implications

438 The suggestion that the St. Lawrence rift faults are inherently weak has broad impli-
439 cations for seismicity of the St. Lawrence as a whole. While monitoring slip along the
440 modeled faults (Figure 10), it is noted that outside of the crater zone, slip is on aver-
441 age evenly distributed along the rift, with the exception of somewhat increased pulses of
442 slip just outside the crater. At any one time, however, only small segments of the faults
443 are active. Based on this model behaviour it can be speculated that slip activity in the
444 St. Lawrence may migrate along strike over time, in which case seismic risk in currently
445 quiescent areas of the rift valley may be underestimated. Seismic hazard maps based on
446 historical seismicity often contain ‘bulls eyes’ of high hazard around areas with recent

447 large earthquakes [*Stein, 2007*]. This may, however, be an artifact of the relatively brief
448 seismic record. To account for the possible temporal migration along regional structures
449 it may be beneficial to employ a more robust approach to hazard estimation using both
450 historic seismicity and recognized regional structures that account for increased estimates
451 between active seismic zones. Such an approach is currently used for hazard maps by the
452 Geological Survey of Canada [*Adams and Atkinson, 2003*].

453 The models also helps to clarify the unusually large range of focal mechanism patterns
454 observed in the CSZ. In particular, the models highlight a possible scale dependence
455 between large and small events, where moderate and large events are more influenced by
456 regional structural trends than their smaller counterparts. This has broad implications for
457 interpreting focal mechanisms at regional scales, particularly in intraplate settings. The
458 models indicate that while stress tensors show little deviation from the applied orientation
459 of S_H , focal mechanisms computed from slip along the weak rift faults produce a P-axis
460 at high angles to the applied stress (Figure 11). Restricting focal mechanisms to only
461 those that occur along the rift faults would therefore result in a misleading estimate of
462 S_H orientation. It is argued that by restricting their dataset to only moderate and large
463 earthquakes, the regional focal mechanism studies of *Zoback [1992b]* and *Du et al. [2003]*
464 introduced a structural bias to events occurring along larger-scale faults, resulting in a
465 substantial apparent stress rotation along the St. Lawrence river ($\sim 60\text{--}90^\circ$, Figure 1).
466 Studies that incorporate smaller magnitude focal mechanisms [e.g. *Adams and Bell, 1991*;
467 *Mazzotti and Townend, 2010*] include events that occur on more variably oriented minor
468 faults. These generally result in average stress orientation estimates closer to the regional
469 field as measured from borehole data, but still with a significant clockwise rotation ($\sim 30\text{--}$

470 45°). The detailed stress inversion results from within the CSZ of *Mazzotti and Townend*
471 [2010] showed that mechanisms from the NW cluster of events yielded a S_H approximately
472 parallel to the regional field. Many of the events in this cluster are located within the
473 central portion of the impact crater (Figure 4a,c). This is notable because the central part
474 of the crater is the region of most intense impact related faulting and fracturing [*Rondot,*
475 1994; *Lemieux et al.*, 2003], resulting in a variably oriented collection of potential failure
476 planes. Results of the models also suggest that the interior of the crater is a region of
477 reduced rift fault slip (Figure 10). The large availability of failure planes as well as the
478 reduced rift fault slip suggest that focal mechanisms in this region would be amongst
479 those least biased by the geometry of the St. Lawrence rift, and thus provide the best
480 local stress field estimates.

481 The large structural geometric bias in focal mechanisms in the St. Lawrence valley lies in
482 marked contrast to many stress inversion results from California and Japan, which are typ-
483 ically consistent with borehole derived stress estimates [*Townend and Zoback*, 2001, 2006].
484 The contrast, however, may be due to a fundamental difference between the seismicity
485 of tectonically active regions versus continental interiors. Since a single stress tensor is
486 capable of reactivating faults in a variety of orientations [*McKenzie*, 1969], stress inversion
487 techniques generally rely on sampling events from many variably oriented structures in a
488 small geometric area to constrain a single stress tensor compatible with all derived slip di-
489 rections [e.g. *Gephart and Forsyth*, 1984; *Arnold and Townend*, 2007]. Tectonically active
490 areas surrounding plate boundaries are characterized by broad deformation at relatively
491 high strain rates; consequently the conditions necessary for stress inversion are easily met
492 and cover large areas. The seismically active faults are also typically geologically young

493 features which formed in the current tectonic regime, and therefore, would be expected to
494 be favorably oriented for reactivation and produce good stress inversions. The conditions
495 in intraplate seismic zones, however, are considerably different. Structures in continental
496 interiors are characterized by significantly lower strain rates than those in tectonically
497 active areas. Inevitably most intraplate regions produce an inadequate number of events
498 to carry out a stress inversion. The few areas where there are sufficient seismic events are
499 often associated with prominent pre-existing weak structure (e.g. a rift zone or aulaco-
500 gen) which formed in a different tectonic regime than what exists today. Under these
501 conditions it is possible that the most prominent structures (i.e the St. Lawrence rift) are
502 poorly oriented for reactivation, although they may be the largest source of weakness.

503 The discrepancy between the focal mechanisms from the rift faults and the regional
504 stress orientation is similar in many respects to plate boundary-related mechanisms in
505 tectonically active areas. Plate boundaries, as opposed to the broad deformation zone
506 around them, are characterized by preferred orientations of faults with low frictional
507 strength, which can be reactivated under very poorly oriented stress conditions. The
508 archetypal example of this is the plate boundary strike-slip San Andreas fault in the San
509 Francisco Bay area California. Here the orientation of S_H in the surrounding crust, as
510 inferred from both borehole measurements and focal mechanism stress inversion is nearly
511 perpendicular to the fault [e.g. *Zoback et al.*, 1987; *Townend*, 2006]. The influence of the
512 plate boundary geometry dominates the overall kinematics, such that the focal mecha-
513 nisms from slip along the fault may give misleading results for use in stress estimates.
514 Consequently, focal mechanisms which are thought to be possible plate boundary events
515 are flagged as such in the World Stress Map database, and are omitted by default from

516 stress maps [*Barth et al.*, 2008]. Off the plate boundary, faults are more varied in orienta-
517 tions and stress inversion results are generally consistent with borehole data [*Townend and*
518 *Zoback*, 2001]. If similar behavior affects the St. Lawrence, it implies that mechanisms
519 within the rift zones with nodal planes consistent with slip along the rift faults should be
520 treated as suspect.

521 The apparent inherent weakness of the St. Lawrence rift raises the question as to
522 whether similar behavior should be expected in other intraplate seismic zones. *Johnston*
523 [1993] noted that there is a global correlation between intraplate seismicity and regions
524 of crustal extension, with about two thirds of events occurring within them. This corre-
525 lation is particularly evident in eastern North America where most of the $M > 6$ events
526 have occurred within the Atlantic and Iapetan rift basins, rifted margin, and aulocagens
527 [*Mazzotti*, 2007]. This correlation is also reflected in the background seismicity (Figure 1).
528 However, unlike the St. Lawrence rift, most events along these other rift structures pro-
529 duce focal mechanisms broadly consistent with the regional stress field [*Zoback*, 1992b;
530 *Du et al.*, 2003]. This consistency may be partially due to the arrangement of structures
531 relative to the stress field. In eastern Canada, for example, besides the CSZ and Lower St.
532 Lawrence which lie along the NE trending St. Lawrence rift, many of the seismic zones lie
533 along NW-SE oriented structures, such as the Ottawa and Saguenay grabens (Figure 1).
534 These structures are approximately perpendicular to the regional orientation of S_H and
535 therefore are optimally oriented to reactivate in the thrust sense, which is prominent in
536 eastern Canada. In the eastern United States paleotectonic rift structures are prominently
537 oriented NE-SW, similar to that of the St. Lawrence. The transition south is also marked
538 by some changes in the regional stress field, including a slight clockwise rotation in S_H to

539 ENE-WSW in the eastern central US, and perhaps more importantly a transition from
540 prominently thrust regime in Canada to strike-slip in the United States (Figure 12). The
541 result is that the stress field is oriented at an acute angle to the major rift faults, which is
542 more favorably oriented for reactivation in a strike-slip sense. The implication is that the
543 apparent consistency between the S_H orientation and P-axes may be due to a serendipi-
544 tous arrangement of weak structures in the stress field that is optimally oriented for fault
545 slip.

7. Conclusions

546 The results of the 3-D stress models of the CSZ agree well with the main findings of the
547 previously published 2-D models [*Baird et al.*, 2009]. Much of the background seismicity
548 patterns can be explained by the intersection of weak faults of the St. Lawrence rift with
549 the damage zone created by the Charlevoix impact. The weak faults modify the pattern of
550 stress around the crater resulting in a stress concentration in the volume between the rift
551 faults within and beneath the crater. In addition to matching broad patterns in seismicity,
552 the 3-D models are able to explain subtle details in the seismicity distribution including
553 the extension of background events to the NE of the crater. The best matching patterns
554 from the models occur when the applied stress field is oriented parallel to the regional
555 field as inferred from borehole breakout data. This suggests that there is no significant
556 local source of stress driving the seismicity; however, to achieve the best calibration, the
557 modeling results require that the rift faults be inherently weak.

558 Modeled slip distribution along the main rift faults in response to boundary displace-
559 ments shows that while slip is distributed throughout the rift, it is locally diminished
560 inside the crater and locally enhanced just outside its boundaries. The area of enhanced

561 slip agrees well with the location of large earthquakes just outside the boundary of the
562 crater. Analysis of the slip vectors of events on the rift fault reveals an inferred P-axis
563 strongly oblique to the regional orientation of S_H , and broadly matching the style of large
564 event focal mechanisms.

565 The models suggest that the inherent weakness of the St. Lawrence rift may be produc-
566 ing a systematic rotation of focal mechanism P-axes relative to the surrounding orientation
567 of S_H . The effect appears to have a greater influence on large events, which preferentially
568 occur along the regional faults, suggesting that small events may provide better indi-
569 cations of the true local state of stress. It is speculated that similar behavior may be
570 expected in other seismically active intraplate rift zones, highlighting a potential caveat
571 for the use of focal mechanisms for stress field estimation in intraplate settings in which
572 seismicity is dominated by large structural features.

573 **Acknowledgments.** We thank Stephane Mazzotti for providing us with an early ver-
574 sion of his manuscript as well as a compilation of focal mechanism parameters. We are
575 grateful for the helpful comments and suggestions of two anonymous reviewers and edi-
576 tor Tom Parsons. Financial support for this work was provided by the Ontario Reseach
577 and Development Challenge Fund, Natural Sciences and Engineering Research Council
578 of Canada Discovery Grants to Steve McKinnon and Laurent Godin, and by an Ontario
579 Graduate Scholarship in Science and Technology to Alan Baird.

Notes

580 1. Animations are available in the HTML.

References

- 581 Adams, J., and G. Atkinson (2003), Development of seismic hazard maps for the pro-
582 posed 2005 edition of the National Building Code of Canada, *Canadian Journal of Civil*
583 *Engineering*, *30*(2), 255–271.
- 584 Adams, J., and P. Basham (1991), The seismicity and seismotectonics of eastern Canada,
585 in *Neotectonics of North America*, edited by D. B. Slemmons, E. R. Engdahl, M. D.
586 Zoback, and D. D. Blackwell, pp. 261–275, Geological Society of America, Boulder,
587 Colorado, United States.
- 588 Adams, J., and J. S. Bell (1991), Crustal stresses in Canada, in *Neotectonics of North*
589 *America*, edited by D. B. Slemmons, E. R. Engdahl, M. D. Zoback, and D. D. Blackwell,
590 pp. 367–386, Geological Society of America, Boulder, Colorado, United States.
- 591 Adams, J., and S. Halchuk (2003), Fourth generation seismic hazard maps of Canada:
592 Values for over 650 Canadian localities intended for the 2005 National Building Code
593 of Canada, *Geological Survey of Canada Open File*, *4459*, 1–155.
- 594 Anglin, F. M. (1984), Seismicity and faulting in the Charlevoix zone of the St. Lawrence
595 valley, *Bulletin of the Seismological Society of America*, *74*(2), 595–603.
- 596 Arnold, R., and J. Townend (2007), A Bayesian approach to estimating tectonic stress
597 from seismological data, *Geophysical Journal International*, *170*(3), 1336–1356, doi:
598 10.1111/j.1365-246X.2007.03485.x.
- 599 Baird, A. F., S. D. McKinnon, and L. Godin (2009), Stress channelling and partitioning
600 of seismicity in the Charlevoix seismic zone, Québec, Canada, *Geophysical Journal*
601 *International*, *179*(1), 559–568, doi:10.1111/j.1365-246X.2009.04275.x.

- 602 Barth, A., J. Reinecker, and O. Heidbach (2008), World Stress Map project guidelines:
603 Stress derivation from earthquake focal mechanisms.
- 604 Bent, A. L. (1992), A re-examination of the 1925 Charlevoix, Québec, earthquake, *Bulletin*
605 *of the Seismological Society of America*, *82*(5), 2097–2113.
- 606 Du, W.-X., W.-Y. Kim, and L. R. Sykes (2003), Earthquake source parameters and state
607 of stress for the northeastern United States and southeastern Canada from analysis of
608 regional seismograms, *Bulletin of the Seismological Society of America*, *93*(4), 1633–
609 1648, doi:10.1785/0120020217.
- 610 Fossum, A. F. (1985), Effective elastic properties for a randomly jointed rock mass, *Inter-*
611 *national Journal of Rock Mechanics and Mining Sciences & Geomechanics Abstracts*,
612 *22*(6), 467–470.
- 613 Gephart, J. W., and D. W. Forsyth (1984), An improved method for determining the
614 regional stress tensor using earthquake focal mechanism data; application to the San
615 Fernando earthquake sequence, *Journal of Geophysical Research*, *89*(B11), 9305–9320.
- 616 Grana, J. P., and R. M. Richardson (1996), Tectonic stress within the New Madrid seismic
617 zone, *Journal of Geophysical Research*, *101*(B3), 5445–5458.
- 618 Hasegawa, H. S., and R. J. Wetmiller (1980), The Charlevoix earthquake of 19 August
619 1979 and its seismo-tectonic environment, *Earthquake Notes*, *51*(4), 23–37.
- 620 Hasegawa, H. S., J. Adams, and K. Yamazaki (1985), Upper crustal stresses and vertical
621 stress migration in eastern Canada, *Journal of Geophysical Research*, *90*(B5), 3637–
622 3648.
- 623 Heidbach, O., M. Tingay, A. Barth, J. Reinecker, D. Kurfeß, and B. Müller (2008), The
624 2008 release of the World Stress Map.

- 625 Itasca Consulting Group Inc. (2005), *FLAC3D (Fast Lagrangian Analysis of Continua in*
626 *3 Dimensions)*, Version 3.0, Minneapolis, MN.
- 627 Johnston, A. C. (1993), Average stable continental earthquake source parameters based
628 on constant stress drop scaling, *Seismological Research Letters*, 64, 261.
- 629 Kumarapeli, P. S. (1985), Vestiges of Iapetan rifting in the craton west of the northern
630 Appalachians, *Geoscience Canada*, 12(2), 54–59.
- 631 Lamontagne, M. (1999), Rheological and geological constraints on the earthquake distri-
632 bution in the Charlevoix seismic zone, Québec, Canada, *Geological Survey of Canada*
633 *Open File*, D3778, 1 CD-ROM.
- 634 Lamontagne, M., and G. Ranalli (1996), Thermal and rheological constraints on the earth-
635 quake depth distribution in the Charlevoix, Canada, intraplate seismic zone, *Tectono-*
636 *physics*, 257(1), 55–69.
- 637 Lamontagne, M., S. Halchuk, J. F. Cassidy, and G. C. Rogers (2007), Significant Canadian
638 earthquakes 1600–2006, *Geological Survey of Canada Open File*, 5539.
- 639 Leblanc, G., A. E. Stevens, R. J. Wetmiller, and R. DuBerger (1973), A microearthquake
640 survey of the St. Lawrence valley near La Malbaie, Quebec, *Canadian Journal of Earth*
641 *Sciences*, 10(1), 42–53.
- 642 Lemieux, Y., A. Tremblay, and D. Lavoie (2003), Structural analysis of supracrustal faults
643 in the Charlevoix area, Quebec: Relation to impact cratering and the St-Laurent fault
644 system, *Canadian Journal of Earth Sciences*, 40(2), 221 – 235, doi:10.1139/E02-046.
- 645 Mazzotti, S. (2007), Geodynamic models for earthquake studies in intraplate North Amer-
646 ica, in *Continental intraplate earthquakes: science, hazard, and policy issues*, *Geological*
647 *Society of America Special Paper*, vol. 425, edited by S. Stein and S. Mazzotti, pp.

- 648 17–33, Geological Society of America, doi:10.1130/2007.2425(02).
- 649 Mazzotti, S., and J. Townend (2010), State of stress in central and eastern North American
650 seismic zones, *Lithosphere*, *2*(2), 76–83, doi:10.1130/L65.1.
- 651 McKenzie, D. P. (1969), The relation between fault plane solutions for earthquakes and
652 the directions of the principal stresses, *Bulletin of the Seismological Society of America*,
653 *59*(2), 591–601.
- 654 Richardson, R. M., and L. M. Reding (1991), North American plate dynamics, *Journal*
655 *of Geophysical Research*, *96*(B7), 12,201–12,223.
- 656 Rivers, T. (1997), Lithotectonic elements of the Grenville Province: review and tectonic
657 implications, *Precambrian Research*, *86*(3-4), 117–154.
- 658 Rondot, J. (1971), Impactite of the Charlevoix structure, Quebec, Canada., *Journal of*
659 *Geophysical Research*, *76*(23), 5414–5423.
- 660 Rondot, J. (1994), Recognition of eroded astroblemes, *Earth-Science Reviews*, *35*(4), 331–
661 365, doi:10.1016/0012-8252(94)90001-9.
- 662 Solomon, S. C., and E. D. Duxbury (1987), A test of the longevity of impact-induced
663 faults as preferred sites for later tectonic activity., *Journal of Geophysical Research*,
664 *92*(B4), 759 – 768.
- 665 Somerville, P. G., J. P. McLaren, C. K. Saikia, and D. V. Helmberger (1990), The 25
666 November 1988 Saguenay, Quebec, earthquake: Source parameters and the attenuation
667 of strong ground motion, *Bulletin of the Seismological Society of America*, *80*(5), 1118–
668 1143.
- 669 St-Julien, P., and C. Hubert (1975), Evolution of the Taconian orogen in the Quebec
670 Appalachians, *American Journal of Science*, *275-A*, 337–362.

- 671 Stein, S. (2007), Approaches to continental intraplate earthquake issues, in *Continental*
672 *intraplate earthquakes: science, hazard, and policy issues*, Geological Society of America
673 *Special Paper*, vol. 425, edited by S. Stein and S. Mazzotti, pp. 1–16, Geological Society
674 of America, doi:10.1130/2007.2425(01).
- 675 Sykes, L. R. (1978), Intraplate seismicity, reactivation of preexisting zones of weakness, al-
676 kaline magmatism, and other tectonism postdating continental fragmentation, *Reviews*
677 *of Geophysics and Space Physics*, 16(4), 621–688.
- 678 Townend, J. (2006), What do faults feel? Observational constraints on the stresses
679 acting on seismogenic faults, in *Earthquakes: Radiated Energy and the Physics of*
680 *Faulting*, edited by R. Abercrombie, A. McGarr, H. Kanamori, and G. Di Toro,
681 Geophysical Monograph Series 170, pp. 313–327, American Geophysical Union, doi:
682 10.1029/170GM31.
- 683 Townend, J., and M. D. Zoback (2001), Implications of earthquake focal mechanisms
684 for the frictional strength of the San Andreas fault system, *Geological Society Special*
685 *Publication*, 186, 13–21.
- 686 Townend, J., and M. D. Zoback (2006), Stress, strain, and mountain building in central
687 Japan, *Journal of Geophysical Research*, 111, B03,411, doi:10.1029/2005JB003759.
- 688 Tremblay, A., B. Long, and M. Massé (2003), Supracrustal faults of the St. Lawrence
689 rift system, Québec: kinematics and geometry as revealed by field mapping and marine
690 seismic reflection data, *Tectonophysics*, 369(3-4), 231–252.
- 691 Zoback, M. D., and M. L. Zoback (1991), Tectonic stress field of North America and
692 relative plate motions, in *Neotectonics of North America*, edited by D. B. Slemmons,
693 E. R. Engdahl, M. D. Zoback, and D. D. Blackwell, pp. 339–366, Geological Society of

694 America, Boulder, Colorado, United States.

695 Zoback, M. D., et al. (1987), New evidence on the state of stress of the San Andreas fault
696 system, *Science*, *238*(4830), 1105–1111.

697 Zoback, M. D., et al. (1993), Upper-crustal strength inferred from stress measurements to
698 6 km depth in the KTB borehole, *Nature*, *365*(6447), 633–635, doi:10.1038/365633a0.

699 Zoback, M. L. (1992a), First- and second-order patterns of stress in the lithosphere: the
700 World Stress Map Project, *Journal of Geophysical Research*, *97*(B8), 11,703–11,728.

701 Zoback, M. L. (1992b), Stress field constraints on intraplate seismicity in eastern North
702 America, *Journal of Geophysical Research*, *97*(B8), 11,761–11,782.

703 Zoback, M. L., and R. M. Richardson (1996), Stress perturbation associated with the Ama-
704 zonas and other ancient continental rifts, *Journal of Geophysical Research*, *101*(B3),
705 5459–5476.

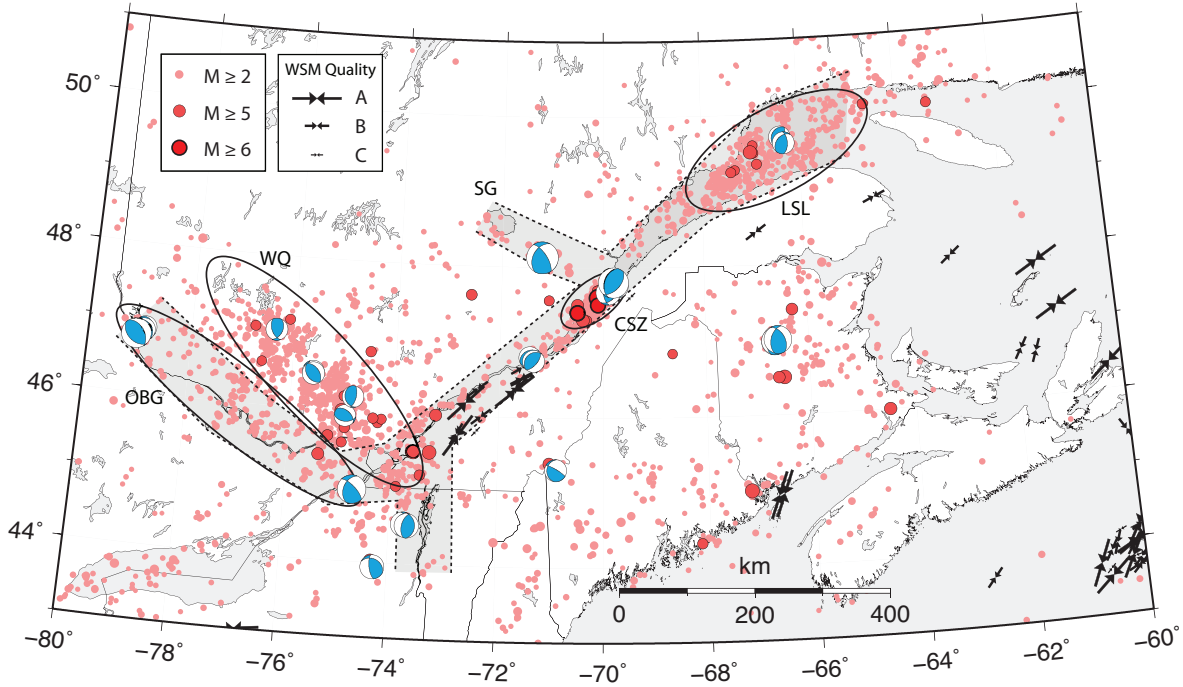


Figure 1. Seismicity and seismic zones in southeastern Canada. Background seismicity (Nuttli magnitude, m_N , ≥ 2 since 1985) from the Geological Survey of Canada, supplemented by large historic events (mostly moment magnitude, M , ≥ 5) since 1663 from *Lamontagne et al.* [2007]. Selected focal mechanisms of moderate to large earthquakes ($M \geq 4.3$) from the compilation of *Mazzotti and Townend* [2010]. Inverted black arrows indicate the orientation of S_H inferred from borehole breakouts from the World Stress Map with quality rankings A ($\pm 15^\circ$ uncertainty), B ($\pm 20^\circ$) or C ($\pm 25^\circ$) [*Heidbach et al.*, 2008]. Shaded grey area indicates the extent of Iapetan rifting [*Adams and Halchuk*, 2003]. Abbreviations: CSZ, Charlevoix Seismic zone; LSL, Lower St. Lawrence; OBG, Ottawa-Bonnechère graben; WQ, Western Québec seismic zone; SG, Saguenay graben.

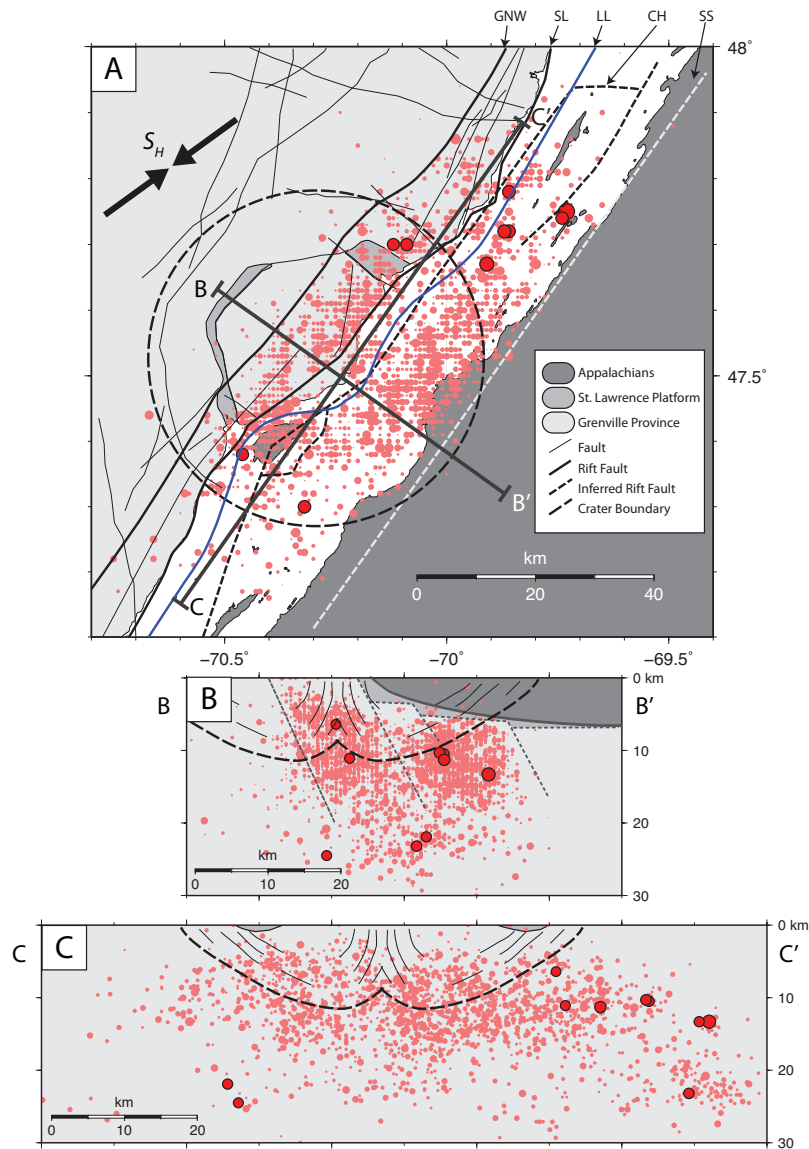


Figure 2. (A) Seismicity and structural geology of the Charlevoix seismic zone. Pink and red circles represent earthquakes with Nuttli magnitudes (m_N) of less than 4.0 or greater than 4.0, respectively. Abbreviations: *GNW*, Gouffre North-West fault; *SL*, Saint-Laurent fault; *CH*, Charlevoix fault; *SS*, South shore fault; *LL*, Logan's line (Appalachian deformation front); S_H , Maximum horizontal compressive stress orientation. Lines B–B' and C–C' refer to cross sections in (B) and (C) (Earthquake data from the Geological Survey of Canada for the period 1985–2009). Cross sectional view of the Charlevoix seismic zone (B) across strike and (C) along strike of the St. Lawrence rift.

Geological structure and crater boundary based on the work of *Lamontagne* [1999] and

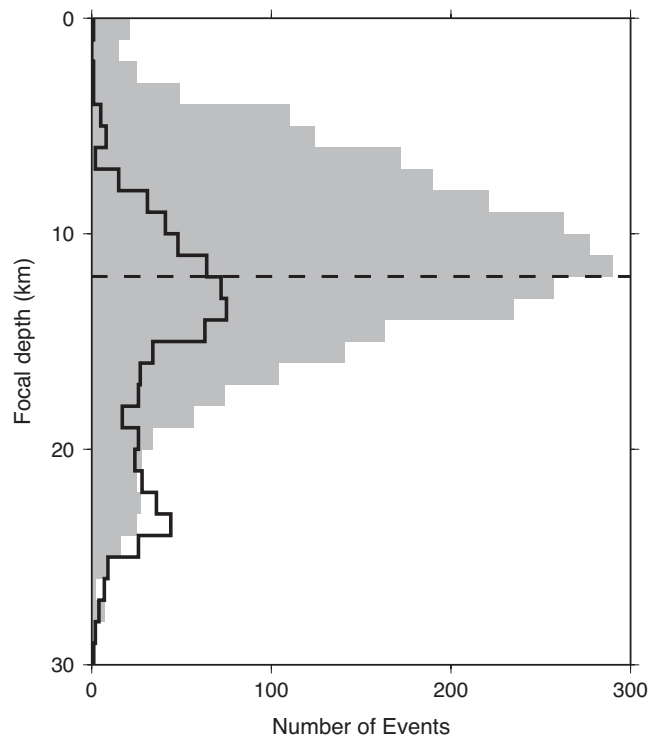


Figure 3. Earthquake depth distribution for events located within or directly below the crater (epicenters within 28 km from crater center, grey) and for the surrounding area (epicenters 28-70 km from crater center, black outline). Dashed line indicates approximate lower boundary of the crater. Data compiled from the Geological Survey of Canada earthquake catalogue.

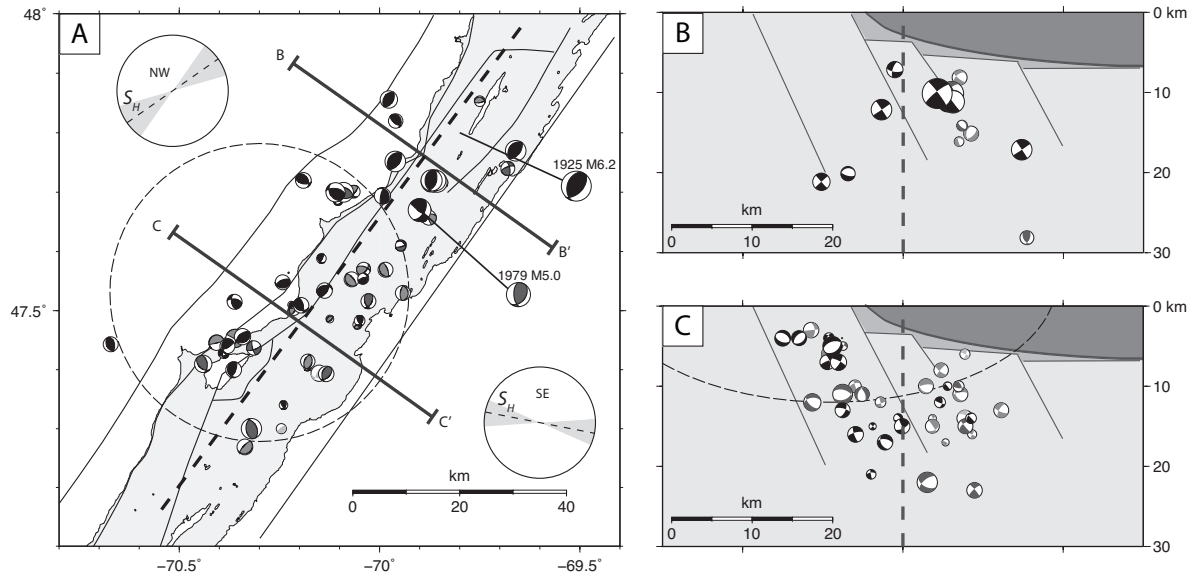


Figure 4. (A) Earthquake focal mechanisms from the Charlevoix seismic zone. Mechanisms are scaled by magnitude. Black, dark grey, and light grey mechanisms refer to quality rankings of A, B, and C, respectively. The two largest events (M 6.2 1925 event and m_N 5.0 1979 event) are indicated. Circles with dashed line and grey angular sectors indicate the average and 90% confidence region of the maximum horizontal compressive stress direction in the NW and SE clusters of seismicity from the stress inversion of *Mazzotti and Townend* [2010]. (B) Cross-section showing mechanisms northeast of the crater. (C) Cross-section showing mechanisms within or below the crater. Thick dashed line indicates the separation of the NW and SE clusters of seismicity used in the analysis.

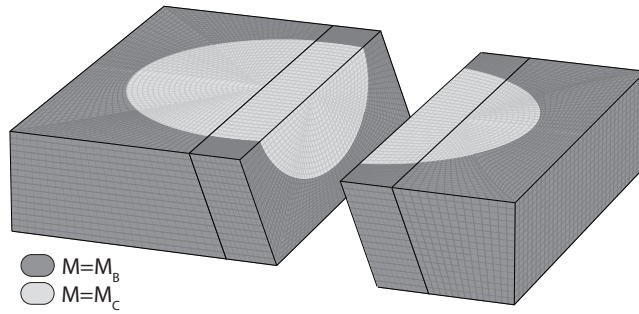


Figure 5. Internal geometry of the model. The crater is represented as an ellipsoid with a horizontal radius of 30 km and depth of 15 km at its center. Rift faults strike at 35° and are steeply dipping to the SE. Colors indicate variations of the elastic moduli (M) in the model between the background rock (M_B) and the weakened crater rock (M_C).

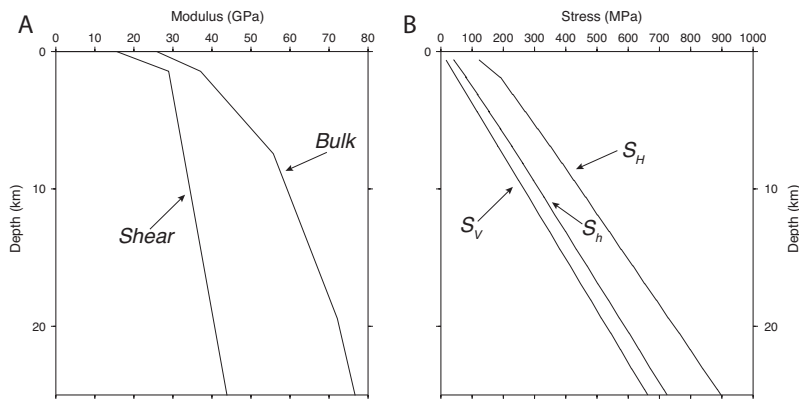


Figure 6. (A) Variation of bulk and shear modulus with depth at a region outside of the impact structure, as computed from the 1-D velocity model in the Saguenay region of *Somerville et al.* [1990]. (B) Final stress profile in region outside on the crater resulting from boundary displacements. S_H , S_h , and S_V refer to the maximum horizontal-, minimum horizontal-, and vertical-stresses, respectively.

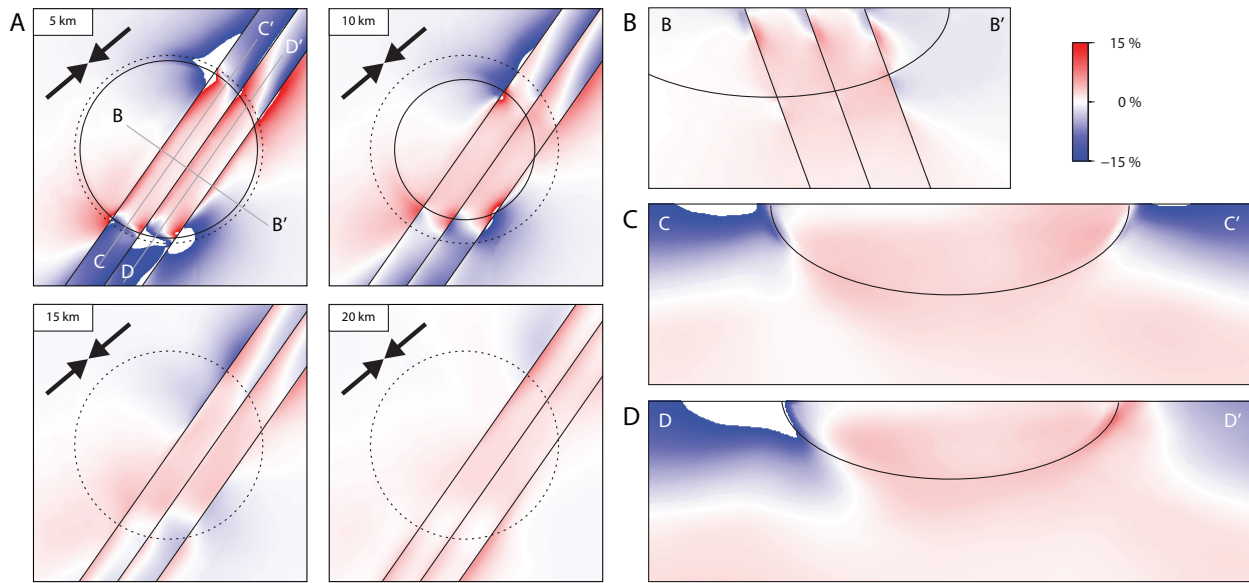


Figure 7. Sectional contour plots showing changes in differential stress relative to the control model using equation 2 for a model with $M_C = 1/4M_B$, a fault friction angle of 5° , and an applied regional S_H orientation of 050° . (A) A series of horizontal depth sections. (B) A cross-section through the center of the crater oriented perpendicular to the rift strike. (C and D) Cross-sections parallel to rift strike, located between the northern and central fault (C), and between the central and southern fault (D).

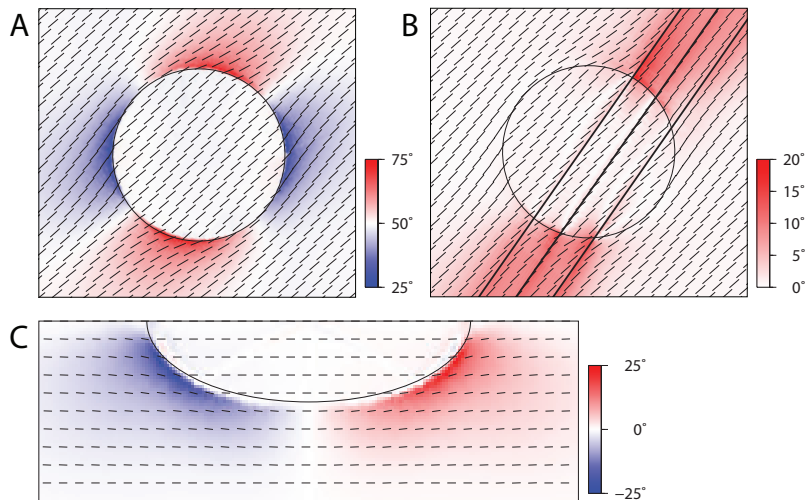


Figure 8. (A) S_H orientation for stress applied to a crater with modulus 1/4 of the background at a depth of 5 km. Applied loading at 50° . (B) Same model as (A) but with weak (5°) frictional faults included, contour plot indicates amount of rotation of S_H relative to locked fault model shown in (A). (C) NW-SE vertical cross-section, showing the deflection of σ_1 orientation beneath the crater.

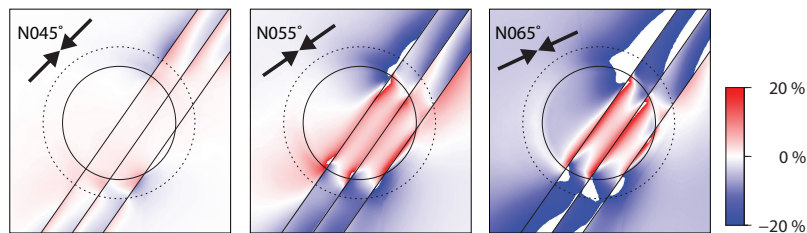


Figure 9. Contour plots of change in differential stress, showing the effect of varying the applied stress orientation.

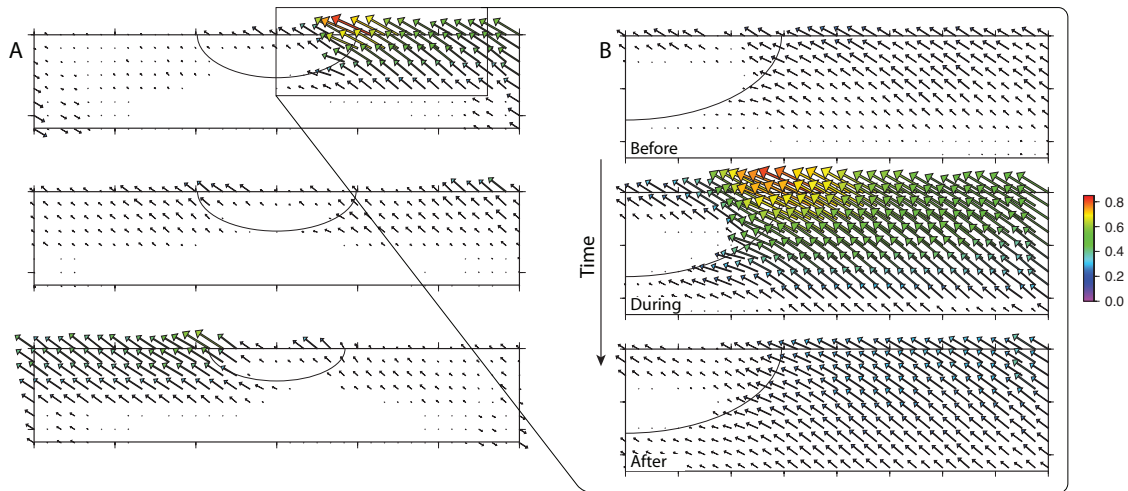


Figure 10. Vector plot showing relative shear displacement of the hanging wall of the rift faults. (A) The northern (top) middle and southern (bottom) faults during one of the pulses of activity just outside the crater. (B) A close-up along the northeastern portion of the north rift fault before, during and after a pulse event. Animations of the behavior can be found in the supplementary material.

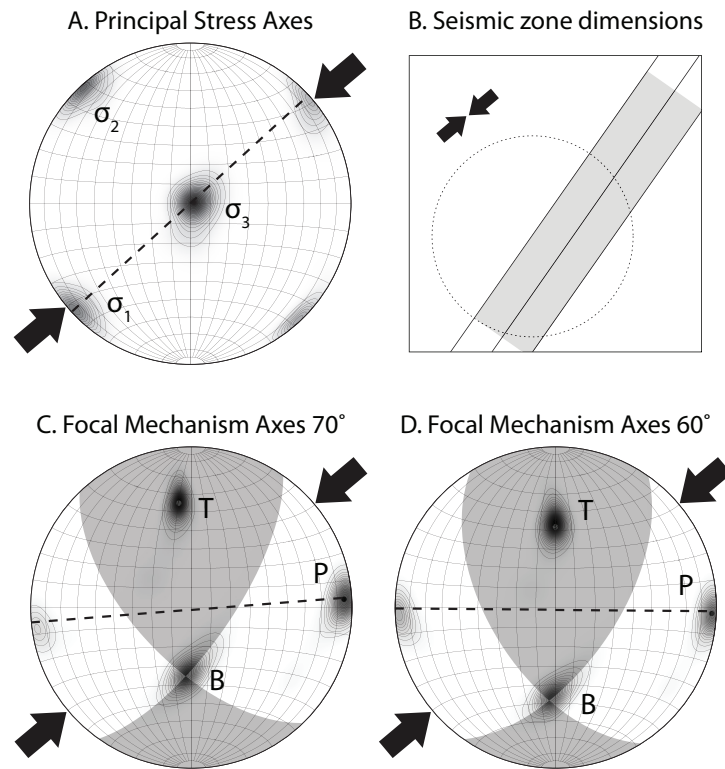


Figure 11. (A) Lower hemisphere stereonet contour plot of the principal stress orientations computed in the model within the upper 15 km of the region defined in (B). (C) The P, T, and B focal mechanism axes calculated using rift-fault slip vectors, with overlaid best fit focal mechanism solution for rift faults dipping at 70°, and (D) best fit focal mechanism for faults dipping at 60°. Large black arrows indicated the direction of loading applied to the model.

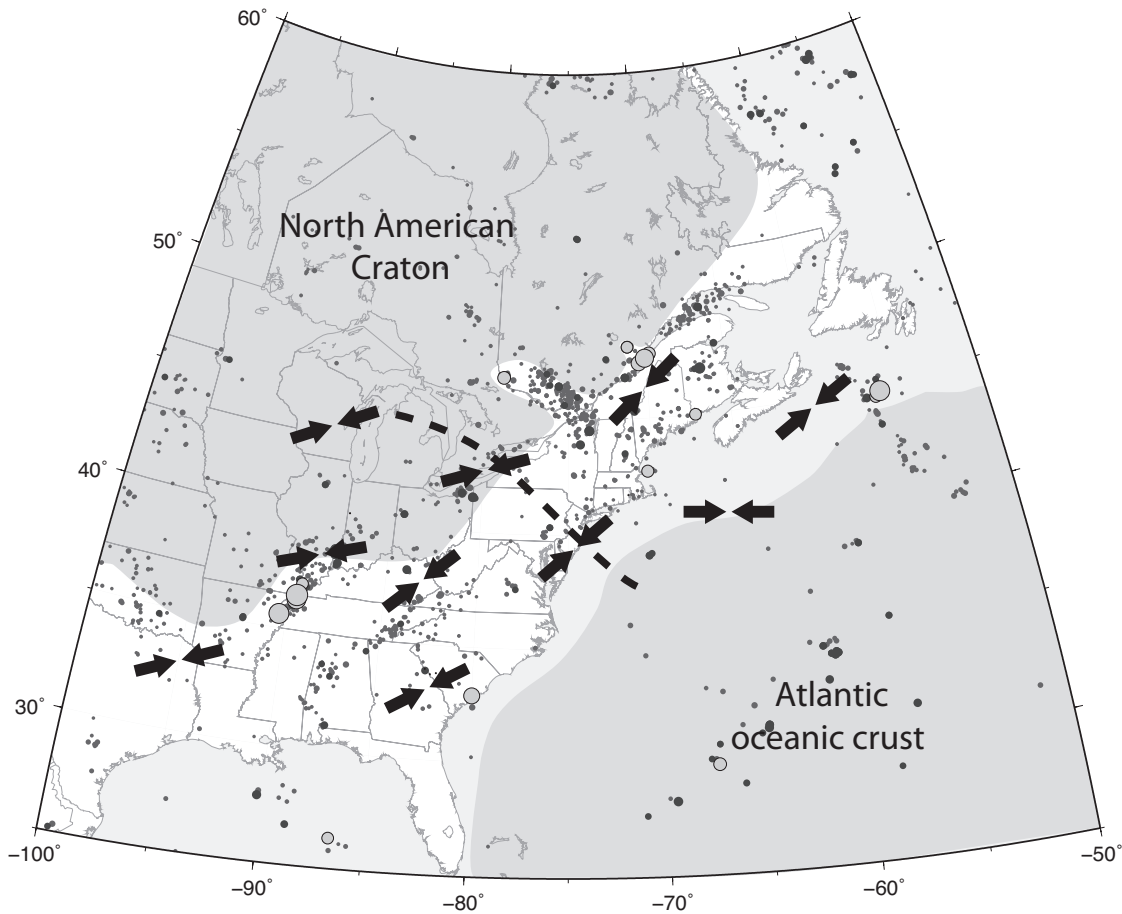


Figure 12. Seismicity and simplified stress map of eastern North America. Background seismicity since 1973 is shown by dark grey ($M \geq 3$) and black ($M \geq 4.5$) circles. Historical large earthquakes (mostly $M \geq 6.0$) are shown by large grey circles. Grey shaded area indicates the low seismicity regions of the North American craton and the Atlantic oceanic crust [modified from *Mazzotti, 2007*]. Inverted arrows show a generalized variation of S_H orientation based on data from the World Stress Map [*Heidbach et al., 2008*]. Dashed line indicates the approximate transition in earthquake focal mechanism style from predominately thrust in the northeast to predominately strike-slip to the southwest [based on the focal mechanism compilation of *Mazzotti and Townend, 2010*]. Seismicity data are from the Geological Survey of Canada and United States Geological Survey catalogues, historic Canadian events are from *Lamontagne et al. [2007]*.